Mattos, Bruno D.; Greca, Luiz G.; Tardy, Blaise L.; Magalhães, Washington L.E.; Rojas, Orlando J.

Green Formation of Robust Supraparticles for Cargo Protection and Hazards Control in Natural Environments

Published in:
Small

DOI:
10.1002/smll.201801256

Published: 19/07/2018

Document Version
Peer-reviewed accepted author manuscript, also known as Final accepted manuscript or Post-print

Please cite the original version:
Mattos, B. D., Greca, L. G., Tardy, B. L., Magalhães, W. L. E., & Rojas, O. J. (2018). Green Formation of Robust Supraparticles for Cargo Protection and Hazards Control in Natural Environments. *Small*, *14*(29), Article 1801256. https://doi.org/10.1002/smll.201801256

Green Formation of Robust Supraparticles for Cargo Protection and Hazards Control in Natural Environments

Bruno D. Mattos, Luiz G. Greca, Blaise L. Tardy, Washington L. E. Magalhães, Orlando J. Rojas**

Dr. B. D. Mattos, L. G. Greca, Dr. B. L. Tardy, Prof. O. J. Rojas
Department of Bioproducts and Biosystems
School of Chemical Engineering
Aalto University
FI-00076, Finland
E-mail: blaise.tardy@aalto.fi, orlando.rojas@aalto.fi

Dr. W. L. E. Magalhães
Embrapa Florestas
Estrada da Ribeira Km 111
83411-000 Colombo, Brazil

Keywords: Self-assembly, nanotoxicology, controlled release, soft chemistry

Alongside important technological advances, nanoparticles have brought numerous environmental and toxicological challenges due to their high mobility and non-specific surface activity. The hazards associated with nanoparticles can be significantly reduced by superstructuring while simultaneously keeping their inherent benefits. In this study, a low temperature and versatile methodology is employed to structure nanoparticles into controlled morphologies from biogenic silica, used as main building block, together with cellulose nanofibrils, which promote cohesion. The resultant superstructures are evaluated for cargo loading/unloading of a model, green biomolecule (thymol) as well as for photo-accessibility and mobility in soil. The bio-based superstructures resist extremely high mechanical loading without catastrophic failure, even after severe chemical and heat treatments. Additionally, the process allows pre- and *in situ*- loading as well as reutilization, achieving remarkable dynamic payloads, as high as 90 mg g^{-1}. The proposed new and facile methodology is expected to offer a wide range of opportunities for the application of superstructures in sensitive and natural environments.

1. Introduction

Alongside increasing technological advances derived from nanoparticles, growing concerns have emerged with regards to toxicological and safety aspects.[1,2] These result from the inherent high surface area to mass ratio of nanoparticles leading to their high mobility across multiple systems, *e.g.*, biological,[3] hydric,[4] and atmospheric.[5] The derived nano-toxicological concerns result mostly from free nanoparticles that interact, bind to and modify the surface properties of exposed biological matter.[6] As a solution to these challenges, colloidal assemblies in the form of superstructures have been proposed, which are able to retain the most desirable properties of the assembled nanoparticles while restricting the mobility of the nanoparticles. In this way the bioaccumulation and non-targeted effects are avoided or minimized. Superstructuring is also used in other fields of science, such as photonics,[7] sensing,[8] energy storage[9] and delivery systems.[10]

The systems available for the formation of supraparticles (SP) in the micro- or macroscales, involve mainly wet-chemistries (e.g. emulsions or controlled aggregation) or assembly in sessile drops. Other alternatives include template-based formation of supraparticles.[11] Wet-chemistries allow fine tuning of the supraparticle architecture but they are more complex and can involve toxic solvents, surfactants or energy-intensive processes. In contrast, the sessile drop technique is considerably less hazardous as it relies on the evaporation-induced assembly of nanoparticles from suspension over superhydrophobic surfaces.[12,13] However, depending on the nanoparticles size distribution, sintering at elevated temperatures (usually > 450 °C) during several hours is needed to ensure SPs with suitable mechanical integrity,[14] making the process energy intensive and limiting tunability of the additional components that can be added. Moreover, it can significantly affect the particles and the potential cargoes. This is especially true when forming SPs from polydisperse building blocks, affecting order and packing and, possibly, impacting negatively the interparticle adhesion. Polydisperse building blocks, however, are often expected and, in fact, may be desirable in catalytic and delivery applications since they endow the system with adjustable porosity and access to the high surface area of the building blocks.[13,14] Techniques to make mechanically robust supraparticles by using simple, soft chemistry-based, methods are highly desirable especially if they are "green" and are able to reduce the health and environmental hazards otherwise associated with nanoparticles.

Here, we demonstrate a versatile and scalable framework for assembling bionanomaterials into morphology-controlled super-strong superstructures. Biogenic silica ($BSiO_2$) particles, used as main building blocks, and cellulose nanofibrils (CNF), introduced to promote interparticle adhesion, were combined into functional assemblies by using a simple, fully aqueous, and low energy strategy (**Figure 1**). Ecofriendly and porous $BSiO_2$ particles, isolated from silicon-accumulating plants through green platforms,[15,16] are in contrast to synthetic porous silica particles obtained from bottom-up processes that generate highly hazardous by-products and toxic intermediate reactants such as ferrosilicon (FeSi) and silicon tetrachloride ($SiCl_4$).[17,18] CNF, derived from mechanical disintegration of cellulosic fibers,[19] represent an emerging alternative for the self-assembly of 3D fibrillar networks, akin to those obtained by chemically-treated aramid (Kevlar) nanofibers.[20,21] The high specific surface area of $BSiO_2$ particles (*ca.* 350 $m^2\ g^{-1}$)[15,16] together with the unique properties of CNF (*i.e.* biodegradability, high aspect ratio and high strength and stiffness)[22] make them an outstanding combination to prepare highly porous and strong superstructures, addressing toxicological and environmental considerations. To test the performance of SPs we used a small biomolecule (thymol) as a model cargo for the assessment of the versatility of the supraparticles formation methodology in terms of loading and unloading.[23–25] The volatile character of thymol was used to evaluate novel pre- or *in situ*-loading strategies as an alternative to the commonly used post-loading. Loading and unloading as a function of the various parameters were measured and the low photo-stability of phenols,[24,26,27] inherent to the thymol molecular structure, allowed quantification of the photo- protection potential of the SPs. Light transmission measurements were used to make a theoretical approximation of the amount of thymol protected from photodegradation as a function of the size of the superstructure. Light accessibility is an important consideration that goes beyond agricultural applications, for example, in photocatalysis. Furthermore, we thoroughly studied the mobility of SPs and nanoparticles in three model soils with distinct physicochemical characteristics.

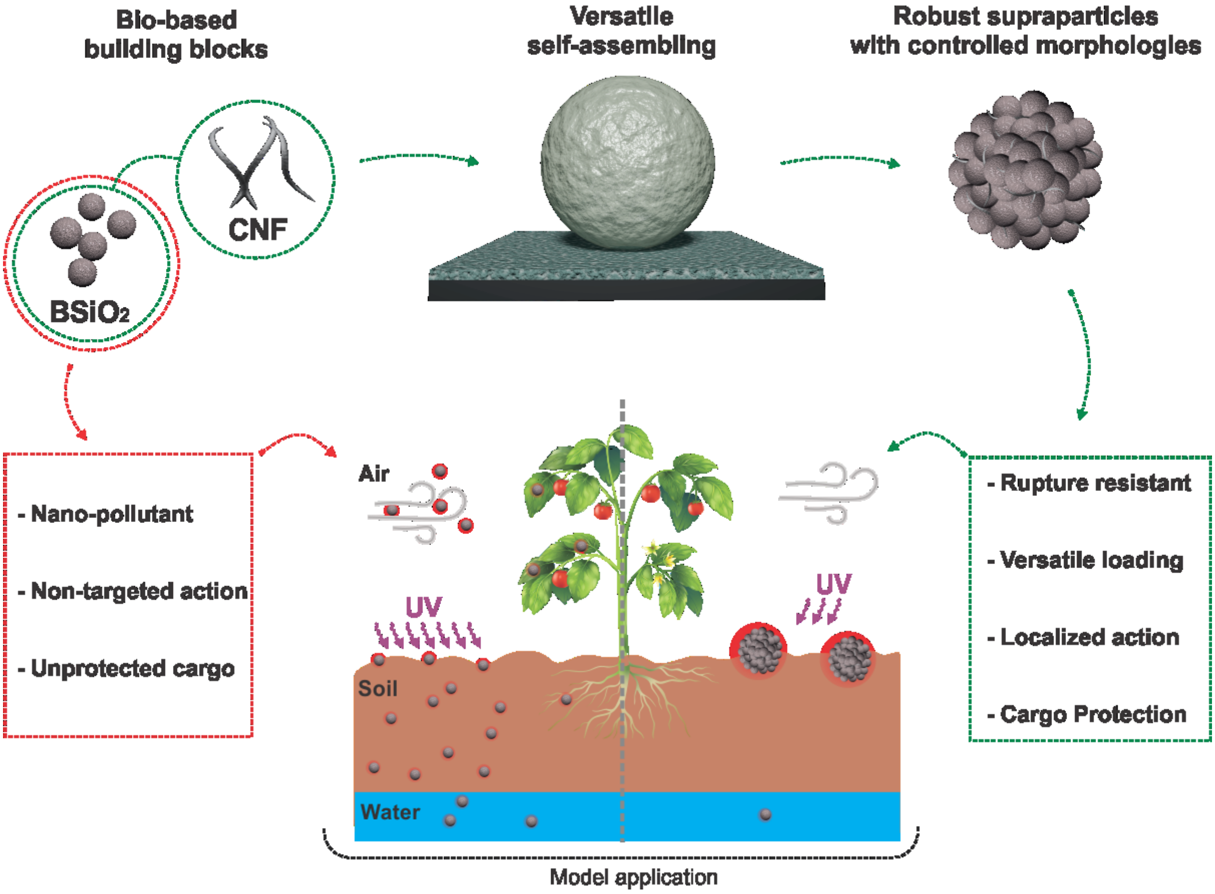

Figure 1. Self-assembly of biogenic silica nanostructures with cellulose nanofibrils to promote interparticle adhesion into super-robust supraparticles (SPs). Demonstration of a model application where the bio-based SPs (right) are used as alternative to free nano- and microparticles (left) to reduce bioaccumulation, increase cargo protection and for sustained biocide release.

2. Results and Discussion

2.1. Superstructures assembly and mechanical characterization

All supraparticles were assembled by evaporation induced self-assembly from aqueous suspensions at 60 ºC and no further processing of particles was necessary to obtain robust assemblies. The process can be also conducted at room temperature where the self-assembly occurs over *ca.* 4 h and results in oblate, but still functional, SPs that were more heterogeneous because of other phenomena occurring over larger time periods such as sedimentation. Spheres or films were obtained by casting the $BSiO_2$-CNF dispersions on the surface of superhydrophobic (immobilized poly(tetrafluoroethylene)) particles or hydrophilic (silanol groups) substrates. Superhydrophobized molds were used for more complex architectures, herein demonstrated through assembly into cylinders (**Figure 2**a). For a given shape, the sizes of the bio-based SPs can be adjusted by exploiting its linear relationship with the volume of the $BSiO_2$-CNF dispersion cast on the substrates (Figures S1a and S1b). Spheres had a higher restriction as far as size. For instance, a 30 µL droplet cast on the super hydrophobic substrate was deformed because of the gravitational force, which made the SP oblate (Figures S1c and S1d). However, the assembled particles were not severely deformed as has been otherwise reported.[14] Furthermore, in the case of SP cylinders and films, the volume of the precursor suspension did not pose limitations in the assembling.

Water evaporation from the $BSiO_2$-CNF suspension was facilitated at 60 ºC. Upon drying, the reduction of free water inside the droplets led to an increased solid fraction in the suspension and, after a short time (typically 10 min) the system self-assembled into packed, highly porous structures (Figure 2b). The formation of a physically entangled CNF network at low solid concentrations was essential to stabilize the $BSiO_2$ particles suspension.[28] This is because CNFs promote multiple physically-driven interactions upon drying induced self-assembly,[28,29] thus resulting in a strong interlocked 3D network that was suitable for physically reinforcing the assembled $BSiO_2$ SPs.

Uniaxial compression tests indicated the robustness of the SPs (Figure 2c), which behaved similarly to spherical granulates.[30] With CNF addition, equivalent to 1 to 5% of the final dry SP solid content, the biogenic silica-based SPs became stronger due to higher adhesion introduced by the fibrils, as indicated by the increasing slopes of the elastic-plastic deformation (zone I) in the force-strain profiles (Figure 2c). With CNF addition, the static force at critical point increased linearly, from *ca.* 0.20 to 1.25 N (Figure 2d). In contrast to what is typically observed for compression of spherical granulates, no abrupt breakage was observed (Figure 2c).

Instead, plateau zones (zone II) with increasing slopes as a function of CNF ratio indicated further reinforcement against crack generation and propagation. This behavior is similar to that reported for fiber-reinforced composites, where fiber debonding and sliding provides an energy dissipation mechanism during crack propagation.[31] The addition of CNF provided effective reinforcement even in the compaction regime (zone III), represented by the exponential portion of the curve (Figure 2c). This exceptional behavior was crucial for reducing or even eliminating the fragmentation at high strains (*ca.* 50 to 60%), which is of great interest for reducing the possible environmental impacts of failed, non-reinforced superstructures resulting in release of high-mobility nanoparticles.

The SPs were submitted to several integrity tests to simulate environmental solicitations as naturally encountered (Figure 2e). Fractured SPs, even if partially, should be avoided as they might behave differently during application and could eventually generate fragments. Therefore, the analysis carried herein concerns the critical load for crack initiation (Figure 2c). The control sample was the non-treated 5% CNF, with a strength of 1.25 ± 0.20 N. The effect of wetting-drying was evaluated after submitting the SPs to five cycles: no notable decrease in mechanical properties (1.1 ± 0.10 N) was observed. In contrast, SPs tested while still wet were considerably weaker, with a fivefold decrease in the critical load (Figure 2e). It is likely that the H-bonds between silica and cellulose as well as between CNF were affected by water competing for such interactions, thus reducing the adhesion in the SPs. Treatment in aqueous media at pH 4 and 9 resulted in similar results: 1.08 ± 0.06 N and 1.24 ± 0.23 N, respectively (Figure 2e). At these pH values the concentration of acid or alkali were not high enough to trigger dissolution or degradation of cellulose or silica. On the other hand, aqueous 1M H_2SO_4 and 1M NaOH promoted drastic changes in mechanical integrity, with a fivefold decrease in strength for the acidic treatment (Figure 2e) and complete failure for the alkali (data not shown). These changes were likely caused by depolymerization of cellulose in acid conditions[32] or silica dissolution[33] and reduced cellulose crystallinity[34] at relatively high NaOH concentration. Thermal treatments – short-term thermal aging (100 ºC for one week) and soaking in boiling water for 1 h – did not significantly affect the mechanical properties of the SPs (Figure 2e). The high chemical and heat resistances of the superstructures highlight the exceptional robustness of the bio-sourced assemblies and offer promise in diverse applications.

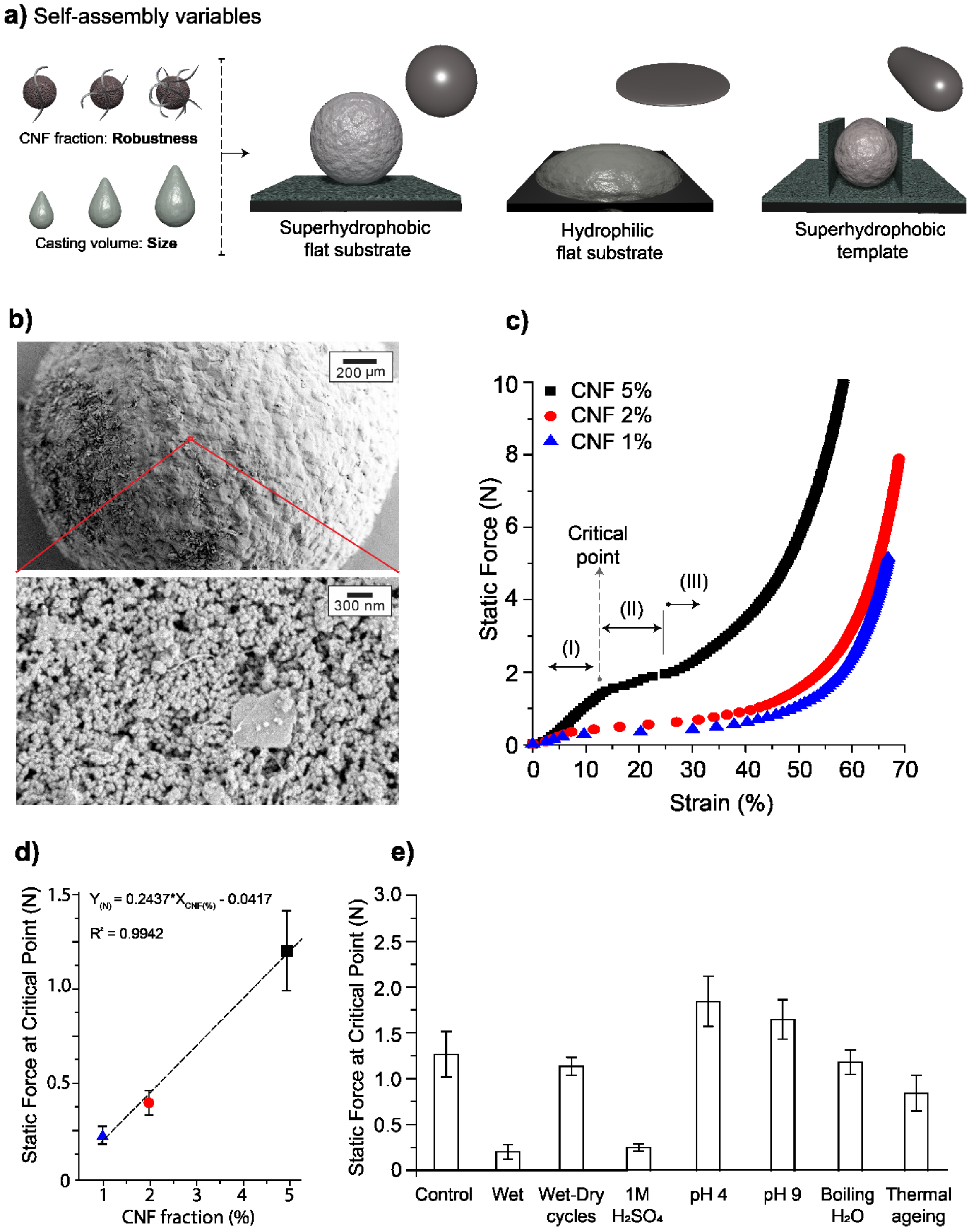

Figure 2. Schematic representation of the factors affecting the size and robustness of the superstructures, as well as the different substrates used to prepare superstructures with

controlled morphologies. Spheres, films and cylinders are obtained by using a flat hydrophobic substrate, a flat hydrophilic substrate or a duct-like hydrophobic template (a). Morphological features of the bio-based superstructures assembled with biogenic silica and cellulose nanofibrils (b). Static force (N) *versus* strain (%) upon compression of biogenic silica-based SPs (spheres with *ca.* 2 mm^3, casting volume of 20 µL) reinforced with CNF solid fractions varying from 1 to 5%, and key zones of the obtained profiles (c). Static force at the critical point as a function of the CNF fraction (d). Compression results after several tests, as indicated, to measure SP's mechanical integrity (static force at the critical point) (e). Note: The given CNF fraction (1 to 5%) refers to the solid content in the final dry SP.

When considering the various SPs applications, cargo loading is critical for impairing functions. In contrast with sintered SPs, which are loaded with temperature-sensitive cargo only by post-loading,[14] pre- or *in situ*-loading strategies were employed herein (**Figure 3**a). The incorporation of the model cargo, thymol, to the biogenic silica SPs, via pre-loading or post-loading, did not significantly affect the mechanical properties (Figure 3b), as the critical load of both methods were just slightly reduced when compared to the unloaded SPs. Conversely, *in situ* loading reduced the critical load to about 50% of the unloaded SPs. Hypothetically, during drying, the dissolved thymol adsorbed at the particle-CNF interface and hindered physical interactions between the hydrophilic surfaces of the fibers and silica, reducing adhesion and overall cohesion. A similar weakening of the interactions might have happened in the pre- and post-loaded SPs, however, to a lesser extent due to the SP assembly and loading order. All the integrity tests, previously described for the unloaded SPs, were performed the same way in the loaded samples and resulted in similar trends (Figure S2).

The different loading strategies, however, resulted in considerable differences in the cargo payload (Figure 3c). Post-loaded cargo was not submitted to any solvent after its incorporation into the SPs, which is not the case of both pre- and *in situ*-loading techniques. Also, the highest payload observed via post-loading is possibly the result of cargo accumulation in macropores of the SPs, derived from the packing constrictions of the irregular-shaped building blocks. The cargo capacity of the pre-loaded SPs was limited by the loading capacity of the building blocks, in this case *ca.* 100 mg g^{-1} of $BSiO_2$.[35] For the pre-loading strategy, a small fraction of cargo was expected to desorb from the loaded-building blocks; however, this small fraction could be retained in the outer layers of the SP. A stronger cargo-carrier interfacial interaction could be an efficient solution to avoid such desorption of the cargo during the self-assembly, as previously reported.[35] The *in situ* methodology resulted in the lowest dynamic payload and loading efficiency (*ca.* 15%). For 90 mg g^{-1} of thymol used, a payload of only *ca.* 12 mg g^{-1} was achieved. Dissolved thymol could have been partially volatilized during drying; also, the shorter incubation period prior to SP assembly may also have led to reduced cargo payload. In addition, the SPs developed with $BSiO_2$ and CNF were amenable to reutilization over five cycles after release, as demonstrated through sequential post-loading and extraction steps. The cargo payload capacity was observed to suffer a slight reduction after the first re-loading, to *ca.* 80 mg g^{-1}. Thereafter, a plateau in loading capacity was observed at 60 mg g^{-1}. These results suggest that some pore obstruction occurred during the recycling steps. After the fifth cycle, 80% of the SPs remained intact (Figure S3a).

In contrast to the effect of loading method, the payload did not significantly change with the CNF fraction, casting volume or morphology of the superstructures (Figure S3b to S3d). This homogeneity in the payload indicated a high pore access of the superstructures, even when the size of the SPs was increased fourfold (diameters from 500 μm to 2 mm). The use of naturally, hierarchically organized $BSiO_2$ as building blocks provided a porous architecture spanning length scales from the micro- (silica smallest units), the meso- (silica smallest units assembling into silica microstructures) to the macro- (resultant silica-CNF superstructures) scales. This led to excellent pore access for both loading and release.

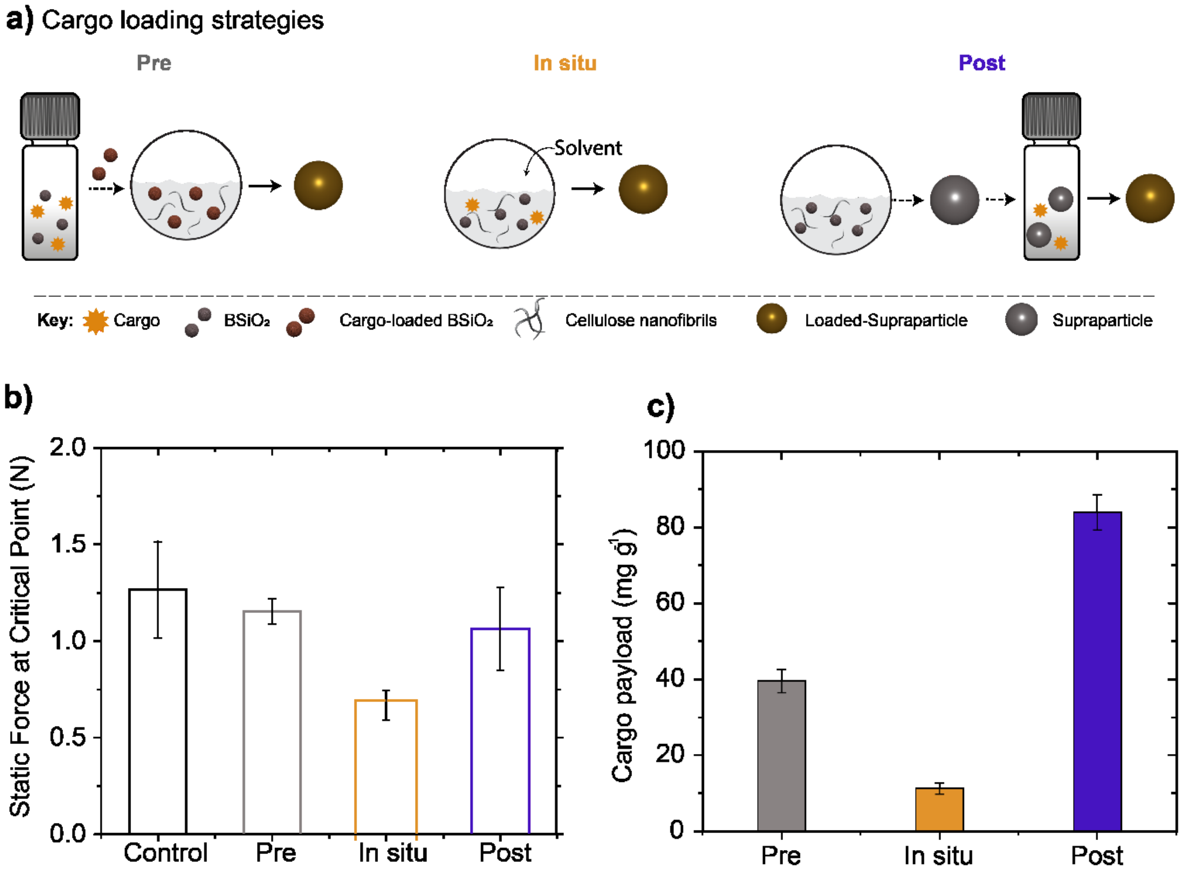

Figure 3. Schematic illustration of the loading methodologies employed to form the bio-based biocidal superstructures, three distinct cargo loading strategies were demonstrated (a). Compression results of the biocidal supraparticles (*ca.* 2 mm^3 SP with CNF fraction of 5%) obtained using different loading methodologies (b). Thymol payload in the superstructured biocides as function of methods for loading (c).

2.2. Release profiles and kinetics considerations

The different strategies applied for biocide loading resulted in similar release profiles (**Figure** **4**b); however, the total amount of biocide released in water was proportional to the initial payload, which varied with loading method (Figure 4a). The amount of thymol released from the SPs was similar to that from the free, suspended nanoparticles (the same used as building blocks in SPs) (Figure S4). This indicates that CNF did not hinder the pore access of the assembled building blocks. In all cases, thymol was released during two distinct stages: initial burst, observed in the first 12 h; followed by slow-release, from 12 to 170 h (Figure 4b). The initial burst release is associated to a higher concentration of cargo on the outer layers of the

SPs. Equilibrium was not achieved for any of the superstructured carriers after 170 h, suggesting a long-term, sustained release.

The mechanisms of cargo delivery was identified by fitting the release profiles to kinetic models.[36–40] Elovich and Korsmeyer-Peppas models described the thymol release reasonable well, but the Elovich model was used to fit the cargo release profile from the SPs, as it provided the best coefficients of determination (over 0.95, Table S1). Elovich fit indicated that the cargo fraction delivered over time (with *k*, the release rate) decreased proportionally to the fractions already released, characteristic of a logarithmical time-dependent behavior.[41] We hypothesize that this mechanism was a result of the highly porous architecture of the SPs that allowed spontaneous flow of the solution into and out of the SPs. In contrast to the molecules adsorbed on the outer shell of the SPs, that were released spontaneously, the molecules deeply incorporated in the particle diffused to the outer regions during the secondary phase. On the other hand, Korsmeyer-Peppas *quasi*-fit provided an indication of anomalous release driven by a complex combination of diffusion and swelling followed by relaxation of the carrier.[42] This release mechanism was a result of the CNF swelling when in contact with water,[43] whereas fibrils can have a six-fold increase in volume,[44] which caused the whole SP to swell.

The release rate coefficient, *k*, was obtained from the slope of the Elovich linearized plot and was used to investigate the delivery performance of the assembled SPs as a function of CNF fraction, size and morphology (Figure 4c, 4d, and 4e). There was a marked effect of the casting volume, at constant solids concentration, on the biocide release rate from the pre-loaded SPs (Figure 4d). The casting volume was strictly related to the SP size. We hypothesize, that the use of pre-loaded building blocks resulted in a more homogenous distribution of biocide across the SP. Thus, the bigger the SP, the longer the diffusion path for the biocide held at the center before reaching the external area. The less marked effect of size on the *k* calculated for *in situ*- and post-loaded SPs suggests a higher concentration of biocide at the outer regions of the SPs, even though there was a tendency for *k* to decrease with the reduced size of the SP

(Figure 4d). Post-loading release rate was nearly unaffected by the size of the particles formed whereas the two other loading strategies resulted in a slower release rate for larger particles. This further suggest the applicability of the developed strategy to tune the cargo release profile. Although, the size dependency on the release rate was significantly less pronounced than for polymeric/drug monolithic dispersion,[45,46] highlighting the conserved porous character of our SPs (Figure 2b).

The surface area-to-volume ratio of bulk delivery systems (*i.e.* non-porous) is key for controlling the release rate of the cargo.[45] Herein, *k* followed the same pattern for all loading methodologies as far as the morphology of the assembled superstructure (Figure 4e). The various morphologies also highlight the possibility to tether the shape of the release systems for various applications.[47] For supraparticles, control over the morphology offers the opportunity to control their mobility in across complex systems as well as their interactions with external environments. For instance, spherical particles are less likely to adhere to surfaces than slab- and rod-like assemblies,[48,49] whereas these assemblies have a higher interfacial contact area. The highest *k* was obtained from the release profiles from films, while the lowest was obtained for the spheres. Considering the same supraparticle volume (mm^3), the "external" surface area ratio of our superstructured systems was *ca.* 1:1.2:5.4 for sphere:cylinder:films. The release rate coefficient followed the same trend but not the same magnitude. For instance, *k* is only 1.4 times higher in the pre-loaded films when compared to the pre-loaded spheres. Thus, the release performance was not strongly influenced by size, CNF fraction or morphology but could be tuned based on loading methodology; making it a versatile approach to assemble homogeneous SPs with well-controlled release properties.

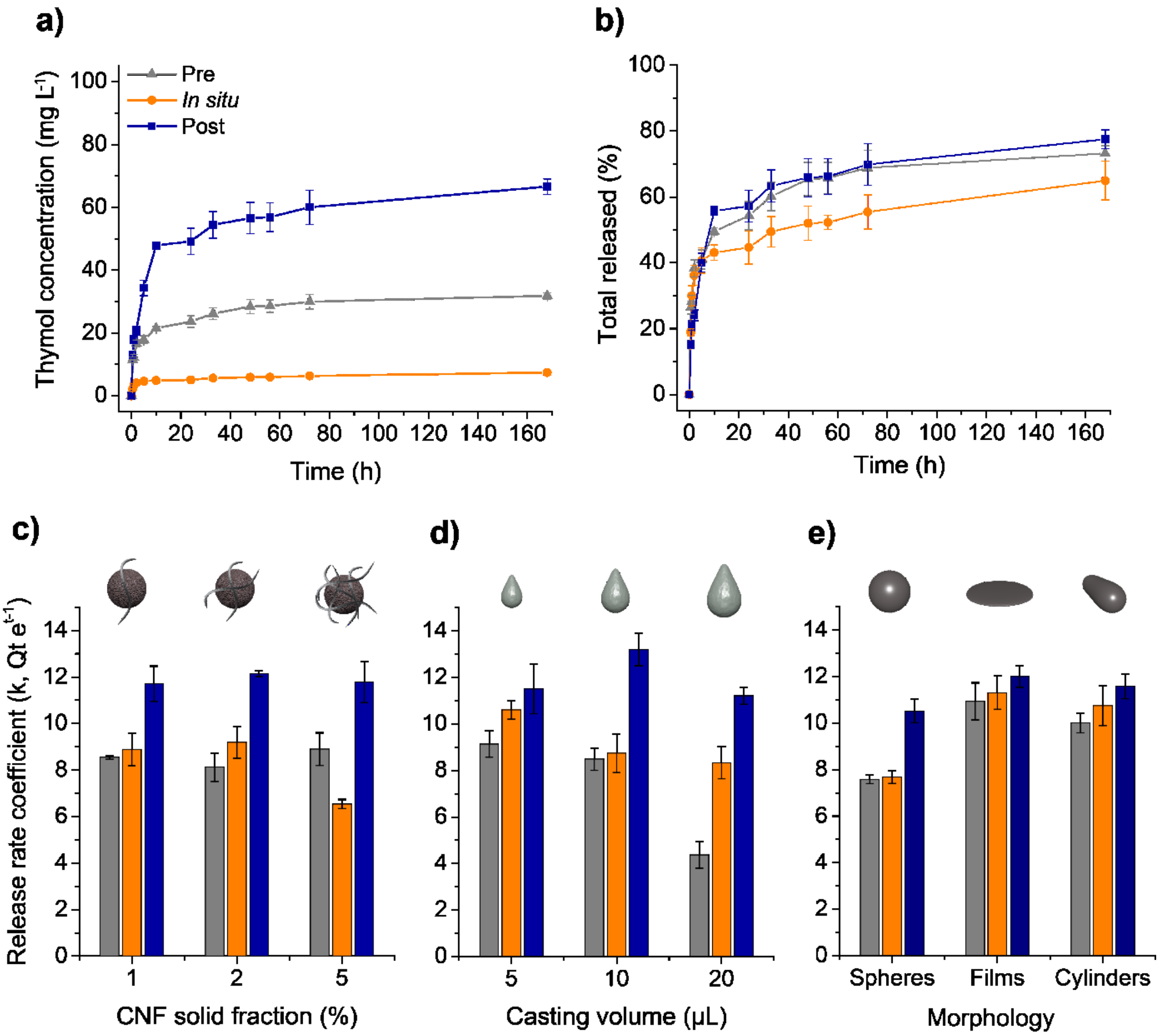

Figure 5. Biocide release profiles as a function of loading methodology and concentration (a) and normalized to the mass of thymol (b). Release rate coefficients, *k*, obtained after linearization of the experimental release profiles using a modified Elovich equation to investigate effects of CNF solid fraction (c), casting volume (d) and morphology (e) on delivery performance. A casting volume of 5, 10 and 20 μL resulted in SPs of *ca.* 0.75, 1.20 and 2 mm^3.

2.3. Cargo protection

The UV-shielding property of amorphous silica has been widely used in many fields of science, such as optoelectronics[50] and textile engineering.[51] UV-shielding is also of great interest to prevent the photodegradation of cargo for delivery applications under high UV, thus increasing their long-term action. Herein, we evaluated thoroughly the photo-protection potential of supraparticles (**Figure 5**a).

We first systematically investigated the fraction of light transmitted through $BSiO_2$-CNF films (CNF fraction: 5%) prepared with gradually increased thicknesses (Figure 5b). Overall, the light transmission in the UV zone was negligible with the thinnest sample (5 μm). This result derives from the polydispersity and also disordered Si-O-Si amorphous arrangement in biogenic silica.[52] In the visible range, the transmittance was *ca.* 35% for the films with 5 μm and it gradually decreased until near zero for the film with a thickness of 150 μm (Figure 5b). A parallel can be drawn from films to spheres. Theoretically, if light penetrates only the outer 150 μm of the whole sphere (Figure 5a and 5b), SPs with diameter of *ca.* 2 mm have *ca.* 85% of the cargo protected against visible light. Consequently, the protection increases in direct relationship with the size of the SP.

Another experimental procedure was carried out to validate the theoretical value for cargo protection (Figure 5c). $BSiO_2$ nano and supraparticles loaded with thymol as well as dissolved thymol as a control were exposed to UV irradiation at 25 ºC. The residual thymol was extracted and measured over time (Figure 5c). Significantly higher fraction of thymol remained in the SPs after 24 h of exposure when compared to both nanoparticles and the thymol solution; respectively *ca.* 100, 60 and 15%. After 72 h, it was observed that 65% of the thymol remained in the SPs, and that the cargo protection was at least twice higher in the SPs when compared to the nanoparticles. The differences in experimental (65%) and theoretical (85%) values can be attributed to simultaneous degradation of thymol triggered by environmental effects (temperature, humidity, generated ozone, oxygen, etc.). This is particularly true as unventilated, high UV intensity considerably increase ozone generation that could diffuse within particles. In addition, a higher concentration of thymol in the outer regions of the post-loaded SPs could be expected, thus leading to a higher degradation than calculated values.

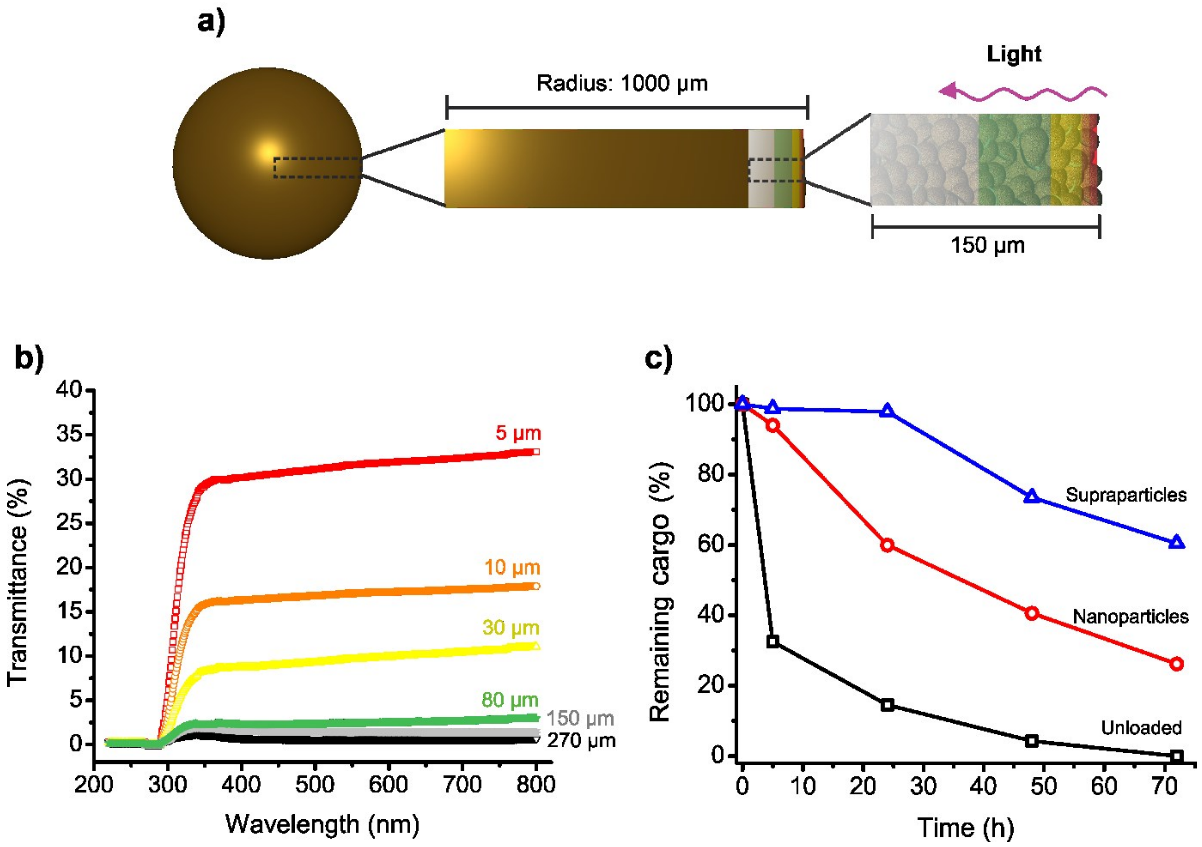

Figure 5. Schematic representation of the supraparticle's zones affected by light (a) as estimated by the maximum light transmittance measured (b). Photodegradation kinetics of unloaded and load thymol under UV exposure (λ_{max} 356 nm) as a function of time (c). The spherical SPs used in the photodegradation assay were *ca.* 2 mm³ in size and contained 5% of CNF by weight.

2.4. Environmental protection

The high mobility of nanoparticles in soil[53] has been a limit to the application of nanoscaled delivery systems in large scale for plant-based applications such as crop protection. In parallel with the bioaccumulation of nanomaterials, nanoparticles can also act as carriers of pesticides and contribute to groundwater contamination. Therefore, herein we compared the mobility of nanoparticles and SPs in model soils using column tests (**Figure 6**a). We selected three soils with different characteristics to investigate factors such as pH, mineral content, density and texture (Table S2) on the particles diffusivity and their potential to contaminate soil. Transmittance measurements of the water outflow were acquired to assess the fraction of particles accumulated along the soil column as well as the leached fraction (Figure S5). The transmittance of the outflow is expected to be inversely related to the solid content in suspension. Aliquots of the outflow were also dried to obtain an approximation of their solid content (Figure 6b).

The behavior of the nanoparticles was linked with the specific characteristics of the soils (Figure 6, Figure S5 and Table S2). The nanoparticles either partially accumulated in the soil or diffused through the column directly to the outflow (Figure 6a). A very high permeability of the nanoparticles in soil A was observed, in which more than 95% of the particles from the inflow diffused directly to the outflow. This soil had very low mineral content and organic matter and was consisting mostly of a packed bed of sand (Table S2). Soil B, rich in positively charged ions (Table S2), retained *ca.* 67% of the inflow solid content along the soil column, representing the highest accumulation. Electrostatic interactions promoted the highest retention of silica nanoparticles, which were negatively charged at or below mildly acidic conditions.[52] Texture was also an important factor in nanoparticles mobility in soil B, as a clay-rich soil, soil B has a higher capacity to promote adhesion of nanoparticles than sandy soils.[53,54] In addition, organic matter present in clay-rich soils plays an important role in the formation of nanoparticles clusters in soils.[55] This result also suggests the benefit in terms of soil contamination from superstructuring. Lastly, soil C had characteristics of both soil A and B, thus behaving intermediately. Retention in the soil or leaching into the groundwater are non-desirable, non-targeted, effects when considering the utilization of particulate delivery systems for crop protection. The levels of retention into soils or leaching into groundwater may depend upon the soil at the application site. It is likely that both of these hazards will happen if nanoparticles were applied directly onto the soil. On the other hand, we showed that biocidal SPs presented very limited mobility in soil regardless of soil type. The percental diffusivity of SP to the outflow was lower than 5%, and the penetration was restricted to only few millimeters on the soil surface (Figure S5a). This behavior is associated with the size of the SPs that significantly reduced their mobility while maintaining the key characteristics of their building blocks.

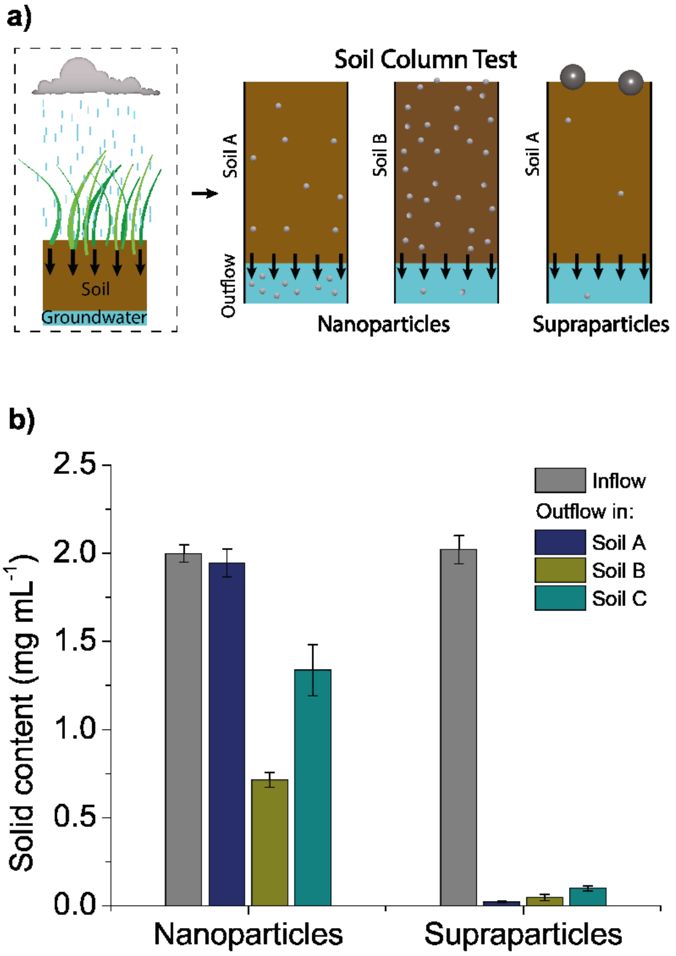

Figure 6. Schematic illustration of the behavior of nanoparticles and supraparticles during soil column tests (a). Comparison between the solid content in the inflow and outflow as a function of soil type (c). The spherical SPs used in the soil mobility test were *ca.* 2 mm^3 in size and contained 5% of CNF.

3. Conclusions

Highly porous, robust superstructures with well-controlled sizes and morphologies could be assembled by using biogenic silica particles as building blocks and cellulose nanofibrils as an adhesion promoter. Biomolecule delivery was evaluated as a model from which several critical factors affecting the general applications of superstructures could be tested. For instance, versatile methodologies were proposed for cargo loading; whereas pre- and *in situ*-loading can now be explored for applications that faced limitations from the high sintering temperatures used in the conventional SPs assembly. The biocide release profiles were shown to be similar to the ones from biogenic silica nanoparticles highlighting the conserved surface area of the nanoparticles without hindrance of access to their surface by solvents. Once loaded in the supraparticles, the model biomolecule was significantly protected against photodegradation, thus confirming the possible use for long-term bioactivity or bioavailability of given cargos. Also, for photocatalytic applications using modified $BSiO_2$ or inherently photoactive particles, optimum supraparticle sizes and morphologies could be designed from the results of the present study with the same SPs preparation methodology. The robustness of the supraparticles was outstanding, even after several, severe, wet-dry cycles, acid and alkali treatments and thermal stresses. Finally, the strategy introduced was shown to have the potential to significantly reduce negative environmental impacts associated with nanoparticles through an improve methodology of the manufacture of SPs. This was possible through a simple suprastructuring methodology relying on the use of 100% bio-based materials and aqueous processing conditions. Considering such advances, it is possible to envision other applications for the formation of porous materials using such building blocks with applications spanning controlled release, separation or catalysis.

4. Experimental Section

Materials: The primary building blocks, biogenic silica particles (BSiO*2*), were isolated from *Equisetum arvense* (horsetail) following a biorefining procedure previously described.[14] CNF, used as adhesion promoter for the superstructure assembly, were prepared by microfluidizing bleached sulfite hardwood (birch) fibers.[56] Thymol (CAS: 89-83-8) was purchased from Sigma-Aldrich and used as a model cargo. Concentrations are reported in weight%.

Generic assembly of bio-based superstructures: The $BSiO_2$ particles were dispersed in deionized water at a particle concentration of 20 wt% and briefly ultrasonicated to form a stable suspension. The initial CNF suspension was prepared at 1.5 wt%. Both suspensions were mixed and diluted to achieve a fixed total solid content of 10% and different $BSiO_2$-to-CNF ratios used to cast and form the various assemblies. The $BSiO_2$-CNF dispersions were homogenized through vortex-ultrasound cycles. For the assembly of the bio-based nanostructures into superstructures, 5 to 20 μL of the $BSiO_2$-CNF dispersions were cast on a flat superhydrophobic substrate placed on a hot plate (60 ºC) and then left to dry. The superhydrophobic substrate consisted of Teflon particles (diameter *ca.* 30 μm) immobilized on the surface of a double-sided tape.

Preparation of supraparticles of given morphologies: Spheres, films and cylinders were prepared to investigate the effects of the external surface area on the release rate of the biocide. These shapes were prepared by casting the dispersions in three different substrates. Spheres were obtained by following the general assembly procedure previously described. The films were prepared by casting the precursor solution on a glass slide. While the cylinders where prepared by casting the suspension on a duct-like polymeric substrate superhydrophobized using a commercial spray (Glaco, from soft 99 corporation). The distance between walls was 1 mm (Figure 2a).

Thymol loading: Three routes were used to load the cargo molecules (thymol) in the superstructures: post-, pre- and *in situ*-loading. Post-loading: the SPs (50 mg), obtained as described in the generic assembly, were incubated for 24 h in 5 mL of thymol solution in n-hexane (20 mg mL^{-1}). The cargo solution was then removed, and the SPs were dried at 80 ºC for 4h. Pre-loading: $BSiO_2$ building blocks were first loaded with thymol following a previously described procedure.[35] Briefly, 200 mg $BSiO_2$ particles were equilibrated for 24 h in 20 mL of thymol solution in n-hexane (20 mg mL^{-1}), followed by centrifugation (2000 rpm for 2 min) and drying (80 ºC for 4 h). The thymol-loaded particles were then used in the assembly of the SPs. *In situ*-loading: This procedure was slightly different from the generic assembly described above. The same steps were followed, but 50 μL of water were replaced by 50 μL of thymol in an ethanol solution at 100 mg mL^{-1} concentration.

Characterization of the superstructured delivery systems: The quantification of thymol loaded in the superstructures was carried by following an already stablished procedure.[35] Briefly, 5-10 mg of SPs's cargo were extracted with 10 mL of absolute ethanol, then the concentration of the ethanolic thymol solution was measured at 275 nm using a UV calibration curve (Figure S6). The morphological features of the SPs were analyzed in a field emission scanning microscopy (SEM, Zeiss Sigma VP, Germany) using an acceleration voltage of 1.6 kV. The samples were firstly coated with a 3 nm platinum layer. The compression strength of the SPs was evaluated using a dynamic mechanical analysis instrument (Q800 from TA instruments). The compression rate was set to 4 N min^{-1} and the acquisition rate was 1 s per point.

Biocide release profiles and kinetic considerations: The thymol release profiles were obtained using deionized water with NaCl at a concentration of 0.5% w v^{-1} at pH 7 and 25 ºC. Thymol-loaded superstructures (200 mg) obtained from different loading methods, CNF ratios, sizes and morphologies were individually submerged in 1 L of NaCl solution as described above. Then, a few superstructures (weighing *ca.* 10 mg) were removed at fixed time intervals, from 0 to 170 h. The amount of non-released thymol was extracted with absolute ethanol and quantified via a UV-Vis absorbance-based calibration curve (Figure S6). The release profiles were acquired using triplicates.

UV protection and light transmission: BSiO$_2$-CNF films with different thicknesses and a CNF concentration fixed at 5% were assembled on a quartz substrate. The thickness of the films was controlled by limiting the casting area, and using BSiO$_2$-CNF dispersions with different solid fractions (from 1 to 10% w v^{-1}). The thickness of the films was evaluated using a caliper or an optical microscope. UV-Vis spectrophotometry was used to systematically measure the fraction of light transmitted through the films. The photo degradation kinetics of unloaded thymol, and thymol loaded in nano- or SPs was carried under UV exposure. The unloaded and loaded systems were placed at 10 cm from an UV lamp (λ_{max} at 356 nm), and samples were taken over time. The amount of remaining, non-degraded thymol was assessed using the methodology previously described for the release profiles.

Nano and SPs mobility in soil columns: The mobility of nano and SPs in soil were compared using column tests. Three different soils (Table S2) were used to investigate important variables such as pH, mineral content and texture on the diffusion of the particles through the column. The procedures were based on a consolidated work[54], but the columns were scaled down to 9 cm, and the nanoparticles suspension was concentrated to 2 g L^{-1}. Each experiment was carried out using individual columns. To evaluate the nanoparticles mobility, the columns were washed with 50 mL of deionized water, and then 50 mL of the biogenic silica particles suspension was passed through. For the SPs evaluation, the soil was washed as before, then 50 mg of SPs were placed on the soil surface and 50 mL of water was passed through. As controls, the soil column was washed and then another 50 mL of deionized water was passed through. The liquid outflow of each experiment was taken in order to quantify the fraction of particles retained in the soil and the fraction leached to the outflow.

First, the outflow was evaluated in a UV-Vis spectrophotometer using transmittance measurements of the liquid in the visible range. The transmittance of the liquid outflow was compared with the transmittance of the initial nanoparticles suspension. Then, the solid content in the outflow was estimated using a gravimetric approach, by taking 25 mL of the outflow and drying at 103 ºC to obtain the solid fraction.

Supporting Information

Supporting Information is available from the Wiley Online Library or from the author.

Acknowledgements

The authors are thankful for the support of the Brazilian CNPq, CAPES, and Fundação Araucária. O.J.R. acknowledges funding from his ERC Advanced Grant #788489, BioElCell. We are also grateful for support by the Academy of Finland's Biofuture 2025 program (project

3D-Manufacturing of Novel Biomaterials 2228357-4) as well as SIRAF. Luiz G. Greca acknowledges funding by Aalto University School of Chemical Engineering doctoral programme. The Academy of Finland Center of Excellence on "Molecular Engineering of Biosynthetic Hybrid Materials Research" (HYBER) and Aalto University Fablab are also appreciated. This work used facilities and technical support of Aalto University OtaNano - Nanomicroscopy Center (Aalto-NMC).

Received: ((will be filled in by the editorial staff))
Revised: ((will be filled in by the editorial staff))
Published online: ((will be filled in by the editorial staff))

References

[1] V. L. Colvin, *Nat. Biotechnol.* **2003**, *21*, 1166–1170.

[2] M. R. Gwinn, V. Vallyathan, *Environ. Health Perspect.* **2006**, *114*, 1818.

[3] P. V. AshaRani, G. L. K. Mun, M. P. Hande, S. Valiyaveettil, *ACS Nano* **2009**, *3*, 279.

[4] A. A. Keller, H. Wang, D. Zhou, H. S. Lenihan, G. Cherr, B. J. Cardinale, R. Miller, Z. Ji, *Environ. Sci. Technol.* **2010**, *44*, 1962.

[5] R. E. Shaffer, S. Rengasamy, *J. Nanoparticle Res.* **2009**, *11*, 1661.

[6] A. Elsaesser, C. V. Howard, *Adv. Drug Deliv. Rev.* **2012**, *64*, 129.

[7] R. C. Hayward, D. A. Saville, I. A. Aksay, *Nature* **2000**, *404*, 56.

[8] M. P. Cecchini, V. A. Turek, J. Paget, A. A. Kornyshev, J. B. Edel, *Nat. Mater.* **2013**, *12*, 165.

[9] A. Magasinski, P. Dixon, B. Hertzberg, A. Kvit, J. Ayala, G. Yushin, *Nat. Mater.* **2010**, *9*, 461.

[10] E. Loiseau, A. Q. de Boiry, F. Niedermair, G. Albrecht, P. A. Rühs, A. R. Studart, *Adv. Funct. Mater.* **2016**, *26*, 4007.

[11] J. W. Maina, J. Cui, M. Björnmalm, A. K. Wise, R. K. Shepherd, F. Caruso, *Biomacromolecules* **2014**, *15*, 4146.

[12] J. Guo, B. L. Tardy, A. J. Christofferson, Y. Dai, J. J. Richardson, W. Zhu, M. Hu, Y. Ju, J. Cui, R. R. Dagastine, I. Yarovsky, F Caruso, *Nat. Nanotech.* **2016**, *11*, 1105.

[13] D.-W. Lee, M.-H. Jin, C.-B. Lee, D. Oh, S.-K. Ryi, J.-S. Park, J.-S. Bae, Y.-J. Lee, S.-J. Park, Y.-C. Choi, *Nanoscale* **2014**, *6*, 3483.

[14] Y. Wang, A. K. Wise, J. Tan, J. W. Maina, R. K. Shepherd, F. Caruso, *Small* **2014**, *10*, 4244.

[15] B. D. Mattos, G. R. Gomes, M. de Matos, L. P. Ramos, W. L. E. Magalhães, *Waste and Biomass Valorization* **2017**, 1.

[16] V. B. Carmona, R. M. Oliveira, W. T. L. Silva, L. H. C. Mattoso, J. M. Marconcini, *Ind. Crops Prod.* **2013**, *43*, 291.

[17] S. Langård, A. Andersen, J. Ravnestad, *Br. J. Ind. Med.* **1990**, *47*, 14.

[18] A. Hobbesland, H. Kjuus, D. S. Thelle, *Occup. Environ. Med.* **1999**, *56*, 625.

[19] Y. Zhang, T. Nypelö, C. Salas, J. Arboleda, I. C. Hoeger, O. J. Rojas, *J. Renew. Mater.* **2013**, *1*, 195.

[20] J. Zhu, M. Yang, A. Emre, J. H. Bahng, L. Xu, J. Yeom, B. Yeom, Y. Kim, K. Johnson, P. Green, N. A. Kotov, *Angew. Chemie - Int. Ed.* **2017**, *56*, 11744.

[21] J. Lyu, X. Wang, L. Liu, Y. Kim, E. K. Tanyi, H. Chi, W. Feng, L. Xu, T. Li, M. A. Noginov, C. Uher, M. D. Hammig, N. A. Kotov, *Adv. Funct. Mater.* **2016**, *26*, 8435.

[22] C. Salas, T. Nypelö, C. Rodriguez-Abreu, C. Carrillo, O. J. Rojas, *Curr. Opin. Colloid Interface Sci.* **2014**, *19*, 383.

[23] A. Marchese, I. E. Orhan, M. Daglia, R. Barbieri, A. Di Lorenzo, S. F. Nabavi, O. Gortzi, M. Izadi, S. M. Nabavi, *Food Chem.* **2016**, *210*, 402.

[24] M. Nuruzzaman, M. M. Rahman, Y. Liu, R. Naidu, *J. Agric. Food Chem.* **2016**, *64*, 1447.

[25] B. D. Mattos, B. L. Tardy, W. L. E. Magalhães, O. J. Rojas, *J. Control. Release* **2017**, *262*, 139.

[26] C. Turek, F. C. Stintzing, *Compr. Rev. Food Sci. Food Saf.* **2013**, *12*, 40.

[27] P. Chowdhury, S. Nag, A. K. Ray, In *Phenolic Compounds - Natural Sources, Importance and Applications*; (Eds: Soto-Hernandez, M.; Palma-Tenango, M.; Garcia-Mateos, M. del R), InTech, Rijeka, 2017.

[28] K. J. De France, T. Hoare, E. D. Cranston, *Chem. Mater.* **2017**, *29*, 4609.

[29] M. Henriksson, L. A. Berglund, P. Isaksson, T. Lindström, T. Nishino, *Biomacromolecules* **2008**, *9*, 1579.

[30] S. Antonyuk, J. Tomas, S. Heinrich, L. Mörl, *Chem. Eng. Sci.* **2005**, *60*, 4031.

[31] M. Y. He, B.-X. Wu, A. G. Evans, J. W. Hutchinson, *Mech. Mater.* **1994**, *18*, 213.

[32] R. Rinaldi, F. Schüth, *ChemSusChem* **2009**, *2*, 1096.

[33] M. Fertani-Gmati, M. Jemal, *Thermochim. Acta* **2011**, *513*, 43.

[34] A. Mittal, R. Katahira, M. E. Himmel, D. K. Johnson, *Biotechnol. Biofuels* **2011**, *4*, 41.

[35] B. D. Mattos, B. L. Tardy, M. Pezhman, T. Kämäräinen, M. Linder, W. H. Schreiner, W. L. E. Magalhães, O. J. Rojas, *Sci. Rep.* **2018**, *ahead*.

[36] J. Liu, X. Zhang, Y. Zhang, *ACS Appl. Mater. Interfaces* **2015**, *7*, 11180.

[37] Z. Yi, H. I. Hussain, C. Feng, D. Sun, F. She, J. E. Rookes, D. M. Cahill, L. Kong, *ACS Appl. Mater. Interfaces* **2015**, *7*, 9937.

[38] B. D. Mattos, O. J. Rojas, W. L. E. Magalhães, *J. Clean. Prod.* **2017**, *142*, 4206.

[39] B. D. Mattos, W. L. E. Magalhães, *Int. Biodeterior. Biodegradation* **2017**, *123*, 174.

[40] X. Xu, B. Bai, H. Wang, Y. Suo, *ACS Appl. Mater. Interfaces* **2017**, *9*, 6424.

[41] S. H. Chien, W. R. Clayton, *Soil Sci. Soc. Am. J.* **1980**, *44*, 265.

[42] R. W. Korsmeyer, R. Gurny, E. Doelker, P. Buri, N. A. Peppas, *Int. J. Pharm.* **1983**, *15*, 25.

[43] S. Ahola, J. Salmi, L.-S. Johansson, J. Laine, M. Österberg, *Biomacromolecules* **2008**, *9*, 1273.

[44] K. Uetani, H. Yano, *Langmuir* **2012**, *28*, 818.

[45] J. Siepmann, F. Siepmann, *Int. J. Pharm.* **2008**, *364*, 328.

[46] M. Matos, B. D. Mattos, B. L. Tardy, W. L. E. Magalhães, O. Rojas, *ACS Sustain. Chem. Eng.* **2018**, *6*, 2716.

[47] J. Xu, D. H. C. Wong, J. D. Byrne, K. Chen, C. Bowerman, J. M. DeSimone, *Angew.*

Chemie Int. Ed. **2013**, *52*, 6580.

[48] L. Tao, W. Hu, Y. Liu, G. Huang, B. D. Sumer, J. Gao, *Exp. Biol. Med.* **2011**, *236*, 20–29.

[49] S. Shah, Y. Liu, W. Hu, J. Gao, *J. Nanosci. Nanotechnol.* **2011**, *11*, 919.

[50] M. A. Correa-Duarte, M. Giersig, L. M. Liz-Marzán, *Chem. Phys. Lett.* **1998**, *286*, 497.

[51] N. Abidi, E. Hequet, S. Tarimala, L. L. Dai, *J. Appl. Polym. Sci.* **2007**, *104*, 111.

[52] B. D. Mattos, O. J. Rojas, W. L. E. Magalhães, *Powder Technol.* **2016**, *301*, 58.

[53] B. Schrick, B. W. Hydutsky, J. L. Blough, T. E. Mallouk, *Chem. Mater.* **2004**, *16*, 2187.

[54] J. Fang, X. Shan, B. Wen, J. Lin, G. Owens, *Environ. Pollut.* **2009**, *157*, 1101.

[55] G. R. Aiken, H. Hsu-Kim, J. N. Ryan, *Environ. Sci. Technol.* **2011**, *45*, 3196.

[56] J. Guo, I. Filpponen, P. Su, J. Laine, O. J. Rojas, *Cellulose* **2016**, *23*, 3065.

Biogenic silica particles and cellulose nanofibrils are combined into functional superstructures. Self-assembly of bionanomaterials into morphology-controlled superstructures is governed by simple suspension-substrate tunable interactions. The given bio-based superstructures are used for cargo release and multiple protection in natural environments. The incorporation of cargo is expanded for pre- and *in situ*-loading methods, resulting in straightforward self-assembly strategies.

Self-assembly, nanotoxicology, controlled release, soft chemistry

Dr. B. D. Mattos, L. G. Greca, Dr. B. L. Tardy, Prof. O. J. Rojas
Department of Bioproducts and Biosystems
School of Chemical Engineering
Aalto University
FI-00076, Finland
E-mail: blaise.tardy@aalto.fi, orlando.rojas@aalto.fi

Dr. B. D. Mattos, Dr. W. L. E. Magalhães
Embrapa Florestas
Estrada da Ribeira Km 111
83411-000 Colombo, Brazil

Green Formation of Robust Supraparticles for Cargo Protection and Hazards Control in Natural Environments

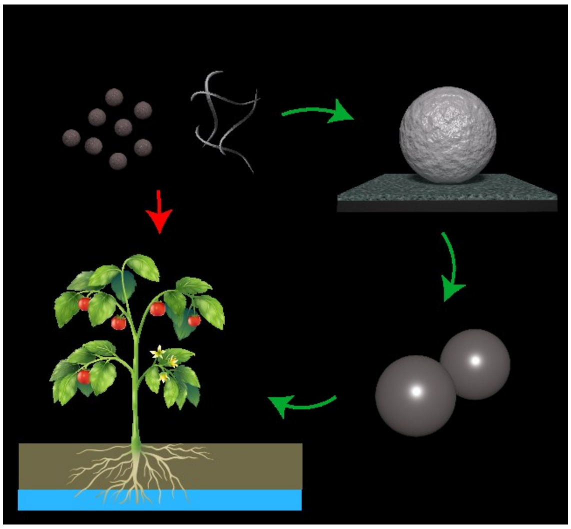

(55 mm broad x 50 mm high)

Supporting Information

Green Formation of Robust Supraparticles for Cargo Protection and Hazards Control in Natural Environments

Bruno D. Mattos, Luiz G. Greca, Blaise L. Tardy, Washington L. E. Magalhães, Orlando J. Rojas**

This supporting information document contains six (6) figures and two (2) tables.

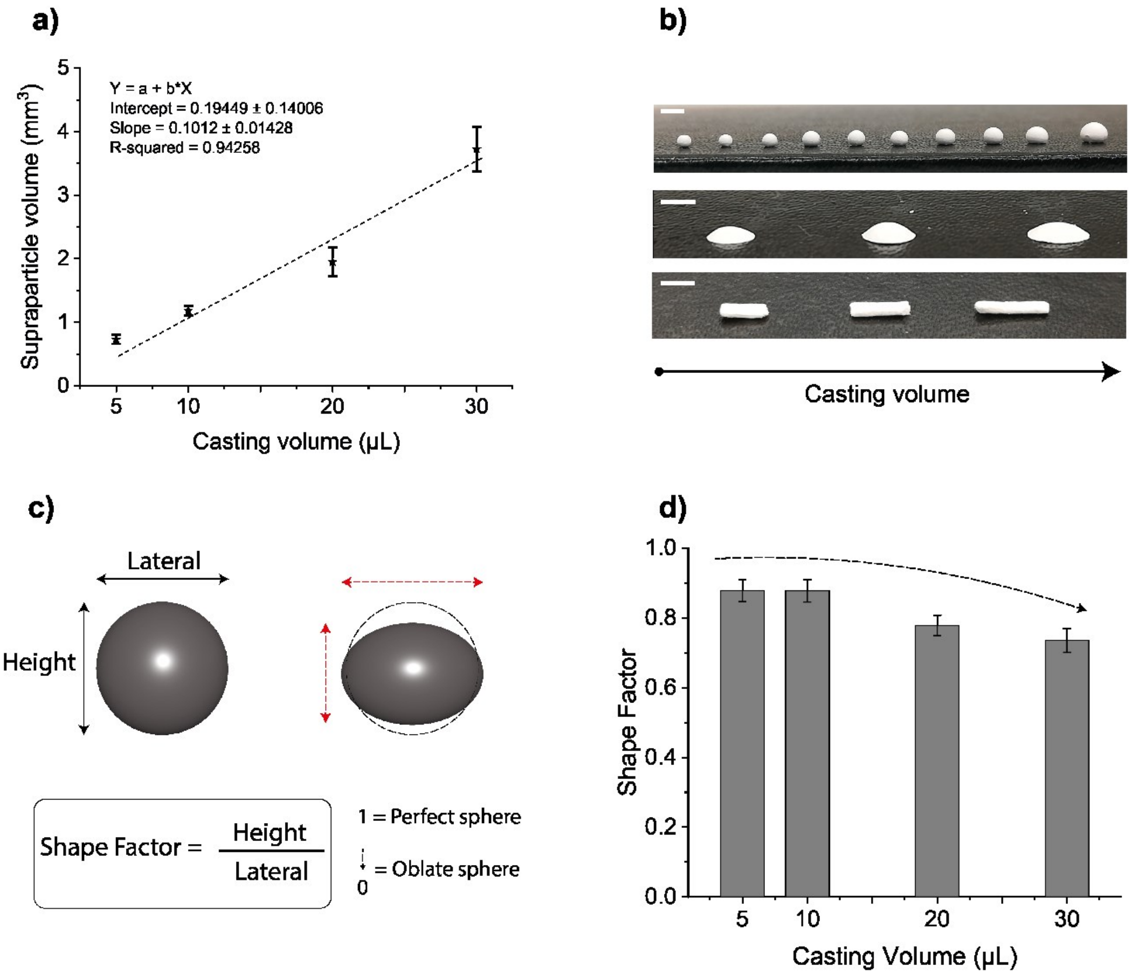

Figure S1. Volume of spherical supraparticle as a function of the casting volume (a). The observed linear relationship in (a) was used to control the supraparticle size (b). A shape factor was formulated (c) to estimate the threshold (d) of the casting volume for the shape transition from spherical to oblate superstructures. Panels "a", "c" and "d" apply directly to spheres.

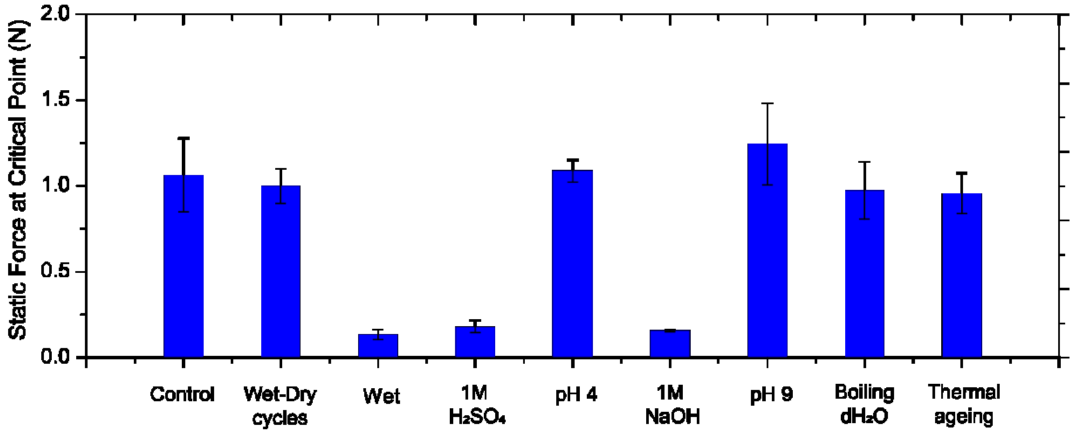

Figure S2. Compression results of loaded SPs after several mechanical integrity tests.

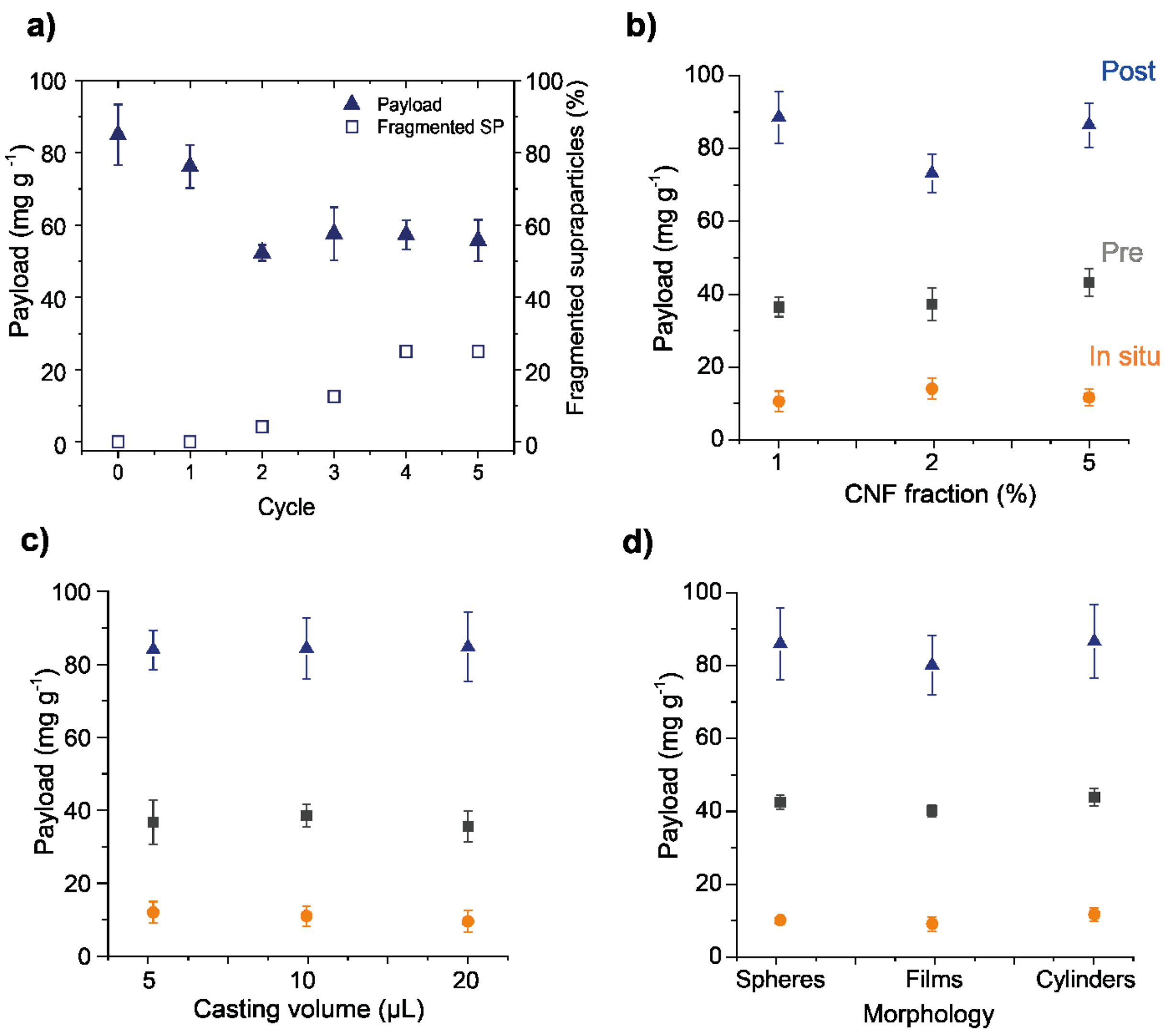

Figure S3. Thymol payload and percent of fragmented supraparticles after five sequential loading, extraction and post-loading cycles (a). Thymol payload as function of CNF fraction (b), casting volume (c) and morphologies (d).

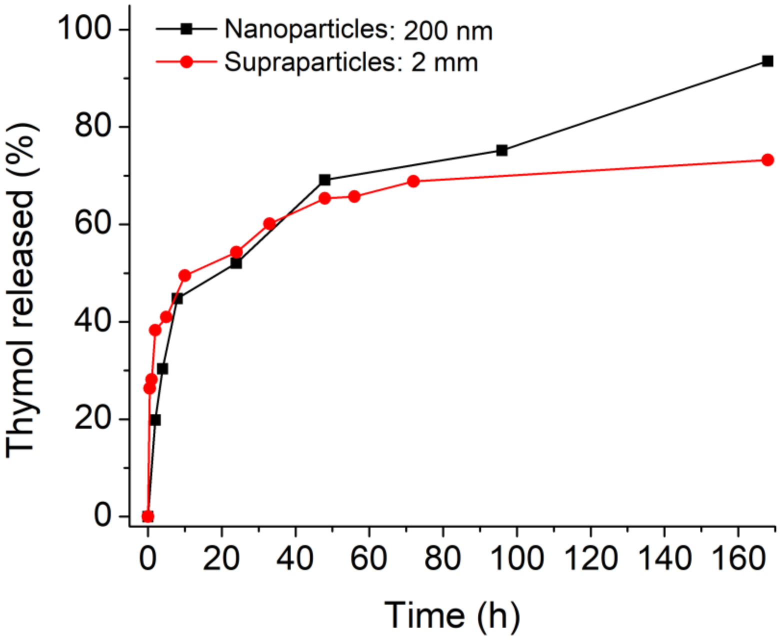

Figure S4. Comparison of the biocide release profiles acquired for the supraparticles (SP with *ca.* 2 mm^3 assembled using 5% of CNF) and the colloidally stable $BSiO_2$ nanoparticles.

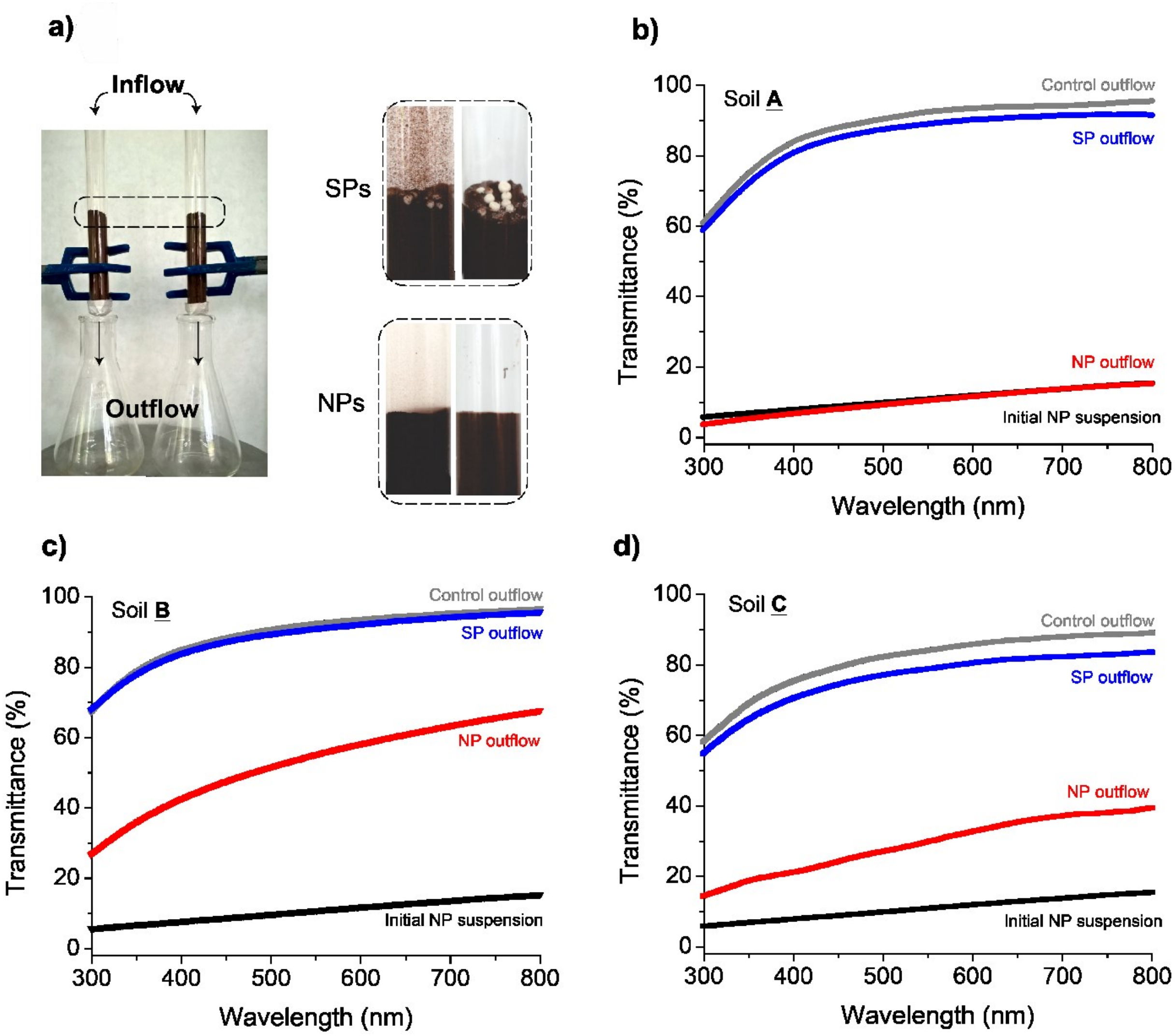

Figure S5. Typical procedure for the investigation of the mobility of particles in soil (a). Transmission spectra acquired in the range from 300 to 800 nm in order to investigate the presence of suspended solids in the outflow obtained after the permeation of the soil column with the nanoparticles suspensions or water (in the case of supraparticles) (b – d).

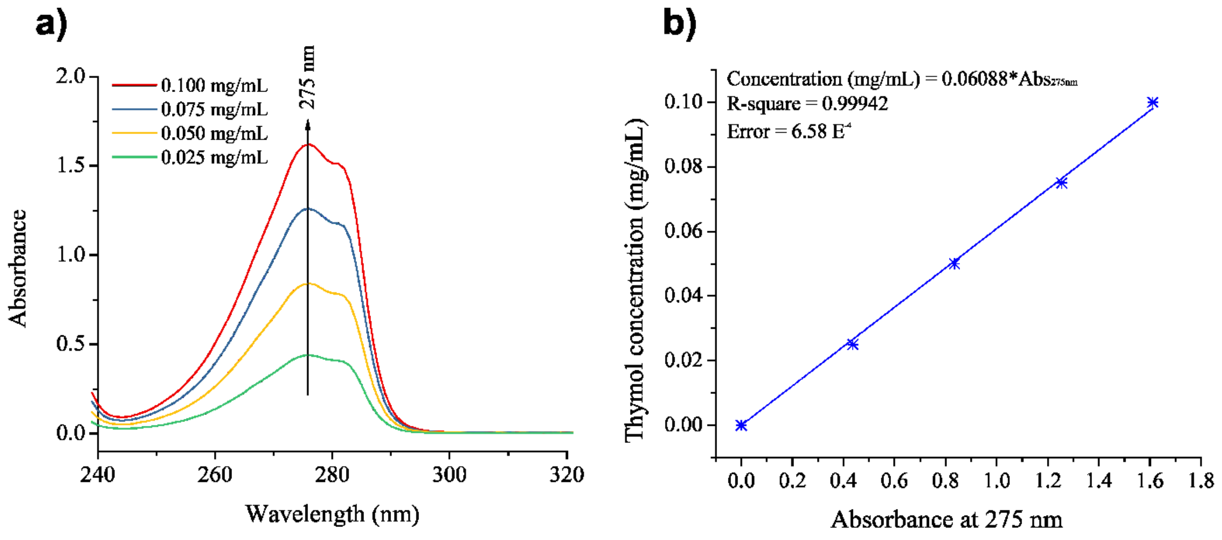

Figure S6. UV spectra obtained for ethanolic thymol solutions (a) in order to build a calibration curve (b)

Table S1. Coefficient of determination of the kinetic models applied as a tentative to explain the release of thymol out from the supraparticles (*ca.* 2 mm³ spheres prepared using 5% CNF)

Model	Equation	Loading Method		
		Pre	In situ	Post
Zero Order	$Q_t = kt$	0.61	0.66	0.54
First Order	$Q_t = e^{-kt}$	0.51	0.48	0.41
Second Order	$1/Q_t = kt$	0.41	0.32	0.3
Parabolic-diffusion	$Q_t = kt^{1/2}$	0.86	0.85	0.8
Korsmeyer-Peppas	$\log Q_t = \log k + n \log t$	0.97	0.89	0.97
Elovich	$Q_t = k\ln t$	**0.98**	**0.95**	**0.97**

Q_t = amount released at time *t*; *t* = time; *k* = release rate constant; *n* = kinetic exponent of the Korsmeyer-Peppas model.

* The equations were presented in their integrated state, considering only desorption and that the initial concentration of the biocide in the release microenvironment was zero.

Table S2. Overall chemical composition, and texture of the soils selected to investigate the mobility of nanoparticles versus their superstructured form.

Soil	pH ($CaCl_2$)	Ca^a	Mg^a	K^a	P^b	C (%)	$Clay^c$	$Sand^c$
A	4.35	0.94	0.03	0.09	44.3	0.61	122	875
B	5.20	9.20	2.80	0.64	3.7	4.77	>600	
C	3.70	0.20	0.10	0.15	2.5	3.51	334	433

Key: $^{a)}$ cmol dm^{-3}; $^{b)}$ mg kg^{-1}; $^{c)}$ g kg^{-1}